Experimental and Numerical Cavitation Flow Analysis of an Industrial Inducer

Y. Bouziad Ait, Mohamed Farhat, Jean-Louis Kueny, Kazuyoshi Miyagawa

Experimental and numerical cavitation flow analysis of an industrial inducer

Author	Firm / Institution	City, Country	Lecturer (x)
Youcef Ait-Bouziad *Mohamed Farhat* *Jean-Louis Kueny* *François Avellan*	*Laboratory for Hydraulic Machines - EPFL*	*Lausanne, Switzerland*	*(x)*
Kazuyoshi Miyagawa	*Mitsubishi Heavy Industry, R&D center*	*Takasago, Japan*	

Abstract

In the present study, a CFD model for cavitation simulation have been investigated and compared to experimental results in the case of 3-bladed industrial inducer. The model uses a multiphase approach, based on multiphase mixture assumption. A truncated form of Rayleigh-Plesset equation is used as a source term for the inter-phase mass transfer. The model allows a good prediction of the cavitation inception as well as the main cavity dimensions. The threshold corresponding to the head drop is also well predicted by the model. It was found that the cavitation induced head drop is mainly due to an increase of energy losses and a decrease of the supplied energy. The hydrodynamic mechanism of head drop is investigated through a global and local analysis of the flow field.

Résumé

Dans le cadre de ce travail une méthode de calcul pour la simulation de la cavitation a été étudié dans le cas d'un inducteur industriel à 3 aubes. Le modèle utilise une approche multiphasique, fondée sur l'hypothèse de mélange homogène. Une forme simplifiée de l'équation de Rayleigh-Plesset est employée comme terme source, et servant de base pour l'échange de masse liquide-vapeur. On a constaté que le modèle permet une bonne prédiction de l'apparition de la cavitation aussi bien que les dimensions principales de la cavité. Le seuil correspondant à la chute des performances est également bien prédit. On a également constaté que l'altération des performances causées par la présence de la cavitation est principalement due à une augmentation des pertes énergétiques et à une diminution de l'énergie fournie par la roue. Le mécanisme hydrodynamique de l'altération des performances est discuté par une analyse globale et locale de l'écoulement.

Introduction

Cavitation phenomenon is still a limiting factor in the design process of hydraulic machines; it is often responsible of erosion, noise and vibration as well as deterioration of hydrodynamic performances. Cavitation is commonly observed when a hydraulic machine operates under off design conditions. A special case of these machines is the inducer. This specific machine which is generally located upstream of the impeller is designed to resist to cavitation and allows the principal impeller to operate in better operating conditions (Ref. 1). Although the use of inducers is frequent today as in petroleum, chemistry and cryogenic rocket fuel industries, several aspect of their operation remain difficult to model, especially in unsteady cavitating regime.

In the last decade, three different approaches have been mainly proposed for leading edge cavitation simulation in hydraulic machinery. In the first approach, called 'interface tracking' model, the cavity interface is considered as a free surface boundary of the computation domain, and the computational grid includes only the liquid phase (Ref. 3). The second approach is based on a pseudo-density function of the liquid-vapor mixture to close the equations system. A Barotropic law relating the pressure to density is mainly proposed (Ref. 12). Recently, a new cavitation modeling through a multiphase mixture model has been introduced, having an additional equation for the volume fraction including source terms to model the vaporization and condensation processes (Ref. 8, 9).

In the case of inducers, Aerospace research has contributed the most significant progress to the knowledge of cavitation flows in inducers. Several researchers have investigated cavitation phenomena and most of the studies are theoretical/analytical (Ref. 4 et 7) or based on quasi 3D Euler resolution for attached cavitation (Ref. 2).

In the present study, we have tested the ability of a recent CFD method to predict the inducer operation in cavitation condition using a multiphase transport-based model. The mass source term in the volume fraction transport equation is provided from a simple form of the RP equation to model the liquid/vapor mass transfer and is a part of the CFX-TASCflow (Ref. 6) commercial software. A brief theoretical formulation of the physical model is given and is tested in the case of a 3 bladed industrial inducer, where cavitation development is compared to the experimental data, and a statement is made regarding to the ability of the model to predict the cavitation development and performances alteration. Analysis is provided concerning the head drop phenomena.

Theoretical formulation and modeling

For the multiphase transport equation-based model, a truncated form of the Rayleigh-Plesset (RP) equation is used and relies on the assumption that thermal and mechanical equilibrium stands between liquid and vapor phases. The RP equation provides the basis for the rate equation controlling vapor generation/destruction, and is implemented through a volume fraction equation with a source term using a multiphase mixture theory. The governing continuity (1) and momentum (2) equation for a classical RANS and homogeneous mixture multiphase flow are described below. Additional transport equation for the inter-phase mass transfer is added for the liquid phase (3):

$$\frac{\partial}{\partial t}(\rho_m) + \nabla \cdot (\rho_m \vec{U}_m) = 0 \tag{1}$$

$$\frac{\partial}{\partial t}(\rho_m \vec{U}_m) + \rho_m (\vec{U}_m \cdot \vec{\nabla})\vec{U}_m = -\vec{\nabla} p_m + \vec{\nabla}(\bar{\bar{\tau}} + \bar{\bar{\tau}}_t) + \vec{M}_m \tag{2}$$

$$\frac{\partial}{\partial t}(\alpha_l \rho_l) + \nabla \cdot (\alpha_l \rho_l \vec{U}_m) = \dot{m}_l = \dot{m}_l^C + \dot{m}_l^V \tag{3}$$

The cavitation model has been implemented based on the use of the Rayleigh-Plesset equation to estimate the rate of vapor production; the formulation listed here is based on the bubble number density development instead of the volume fraction. For a vapor bubble nucleated in a surrounding liquid the dynamic of the bubble can be described by the RP equation (Ref. 5). This nonlinear ordinary differential equation is difficult to implement within an Eulerian-Eulerian framework for multiphase flows, therefore a first order approximation is used:

$$\dot{R} = \sqrt{\frac{2}{3}\frac{|p_v - p|}{\rho_l}} \tag{4}$$

$$\dot{m}_l = N \rho_l 4\pi R_0^2 \dot{R} \tag{5}$$

Where R is the radius of the bubble, pv the vapor pressure in the bubble, p the pressure in the surrounding liquid and ρ_l the liquid density. The number of bubbles per volume unit of the mixture, N, available as nucleation sites respectively during vaporization and condensation is given by:

$$N^V = \frac{3\alpha_g(\alpha_w + \alpha_g)}{4\pi R_0^3} = \frac{3\alpha_g \alpha_l}{4\pi R_0^3} \tag{6}$$

$$N^C = \frac{3\alpha_v}{4\pi R_0^3} \tag{7}$$

In practice, the vaporization and condensation processes have different time scales. Empirical constants, FC and FV, are introduced to allow for these constraints. The definition of N changes depending on the direction of the phase change.

$$\dot{m}_l^V = -F^V \; 4\pi \; \rho_v \; R_0^2 \; N^V \; \sqrt{\frac{2}{3} Max\left(\frac{p_v - p}{\rho_l}, 0\right)} \tag{8}$$

$$\dot{m}_l^C = \; F^C \; 4\pi \; \rho_v \; R_0^2 \; N^C \; \sqrt{\frac{2}{3} Max\left(\frac{p - p_v}{\rho_l}, 0\right)} \tag{9}$$

The non-condensable gas, assumed as spherical bubbles, provide nucleation sites for the cavitation process. The default value for y_g is taken equal to 10^{-5} and a typical initial radius for the nuclei as $R_0 = 10^{-6}$m. Since no reliable data is available to use for the source terms, we have used a simple and well documented 2D hydrofoil case study to derive optimized values,

which allows the best prediction of cavity dimensions (see Ref. 10 and 11). We have chosen $F^V = 50$, for vaporization (p_v-$p > 0$), and $F^C = 0.015$ for condensation (p_v-$p < 0$).

Inducer case study

Experimental setup

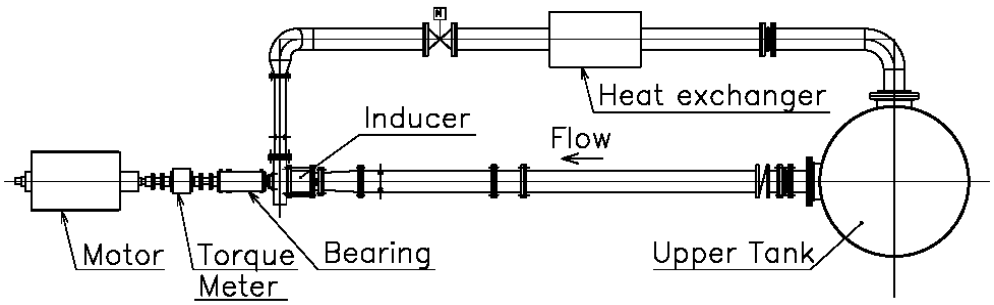

Figure 1 Inducer Test Loop Facility

The present case study refers to a 3-bladed industrial inducer. Measurements of hydraulic performances as well as cavitation visualization have been achieved in the test rig of Mitsubishi Heavy Industry R&D center (Figure 1). In this closed loop, a large number of hydraulic conditions have been tested.

Numerical method

The CFX-TASCflow commercial code, which is used for the present work is a three-dimensional structured mesh code that solves the Reynolds-averaged Navier-Stockes equations with a finite volume method. The solver employs algebraic multigrid method and is fully coupled, momentum and continuity equations being solved simultaneously. A central second-order scheme associated with a modified interpolation coefficients is used for the convection term. Steady state solutions were obtained for different regimes by setting the flow rate at the inducer inlet and the average static pressure at its outlet for the boundary conditions. Single channel geometry in rotating frame of reference is used and periodicity conditions are applied to the channel connections. A k-ε turbulence model is used for the numerical simulations.

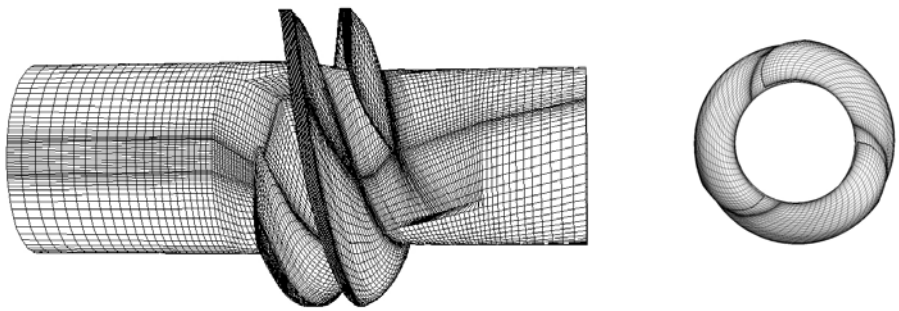

Figure 2 Inducer grid topology

A multiblock structured mesh is generated with the help of TurboGrid mesh generator for hydraulic machines. 6 different meshes using between 150.000 and 500.000 nodes are tested in cavitation free condition and shows no grid influence in term of the head evaluation and the pressure distribution on the blade from 260'000 nodes mesh. This mesh is used for the rest of the computations. The computing domain which corresponds to a single blade to blade passage, 1/3 of the impeller, is made of 9 O-blocks and H-blocks as well as 3 evolution layers of cells in the meridian, hub-to-shroud and blade-to-blade directions to ensure good grid orthogonality and cells evolution factor (Figure 2).

Results

Cavitation visualization corresponding to 3 values of cavitation specific energy coefficient ψ_c are reported Figure 3. Where ψ_c is defined as

$$\psi_c = \frac{2NPSE}{\omega^2 R^2},$$

NPSE, being the net positive suction energy according to IEC 60193 definition.

The cavitation inception is observed for ψ_c=0.6, which corresponds to the numerical prediction. Nevertheless, while the experiment shows a simultaneous inception of cavitation in the tip clearance region and in the leading edge, the simulation predict cavitation inception only in the tip clearance region for ψ_c=0.6. The occurrence of the leading edge cavitation is predicted at ψ_c<0.4 (Fig. 3a and 3b). For values of ψ_c <0.15, cavitation extends to the channel region and reaches the throat leading to a flow blockage (Fig. 3c). The corresponding flow visualization clearly shows strong unsteadiness of the cavity dynamics.

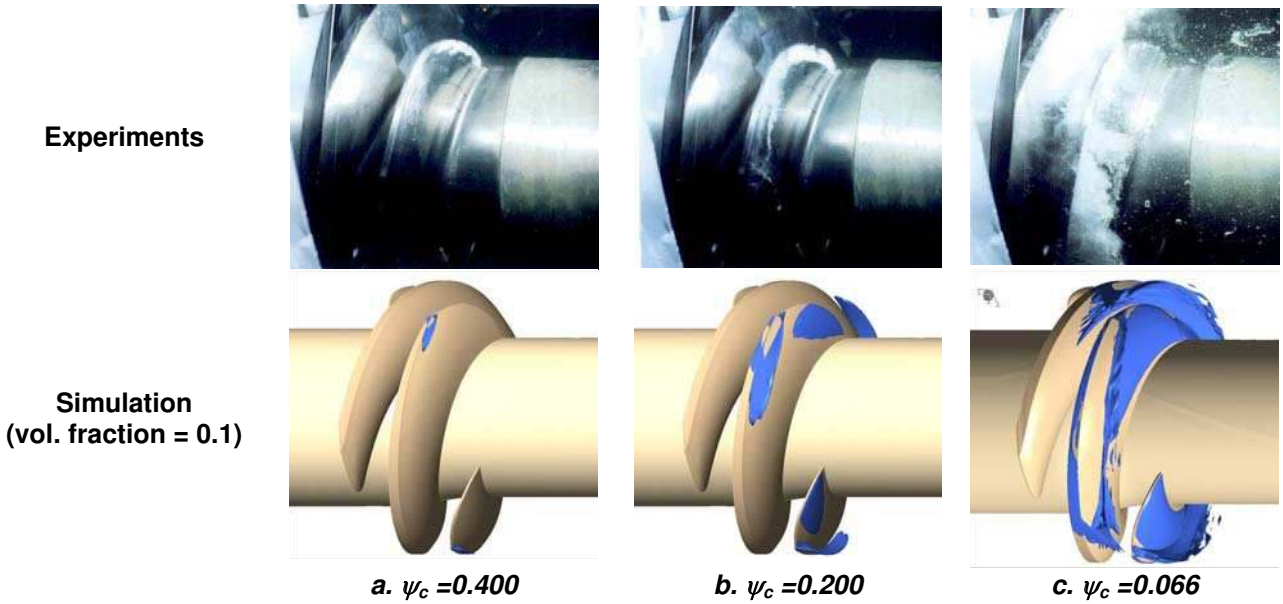

Figure 3 Cavitation development for different ψ_c

We have plotted in Figure 4, the specific energy coefficient ψ as a function of the cavitation number ψ_c, ψ being defined as

$$\psi = \frac{2E}{\omega^2 R^2}$$

Experimental results are compared to the predicted ones and show a good agreement with respect to the threshold of ψ alteration corresponding to ψ_c ~ 0.12. It should be noticed that the suction side cavitation development extends beyond the throat and an attached cavitation is observed in the pressure side when ψ is altered.

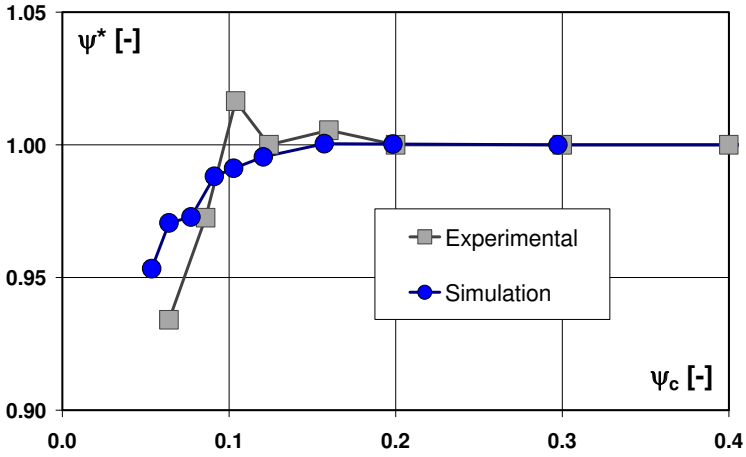

Figure 4 Comparison of experimental and numerical $\psi^* - \psi_c$ *cavitation curves* $\psi^* = \frac{\psi}{\psi_{\text{cavitation free}}}$

The predicted breakdown value agrees well with experimental results when it comes to the beginning of performances drop. For lower values of cavitation numbers, the predicted drop is underestimated. For these flow regimes, the unsteady character of the flow is not taken into account by the flow model.

Energy balance

The energy loss due to the cavitation development is determined by comparing E_t the supplied energy by the inducer to the flow with E_b the specific energy transferred to the fluid by the inducer stage. This is expressed by:

$$E_b = E_t - E_r \qquad (10)$$

where E_r represents the specific energy losses.

Supplied specific energy : The specific energy supplied by the inducer is defined by :

$$E_t = \frac{\vec{T}_t \cdot \vec{\Omega}}{\rho Q} \qquad (11)$$

where $\vec{\Omega}$ is the angular rotation speed and $\vec{T}_t$ stands for the resulting moment of the flow forces acting on the inducer and may be derived from integration of the pressure and the viscous forces on the blades and the hub surfaces.

Inducer energy : The energy E_b transferred to the fluid is defined by the energy balance between the low pressure and high pressure section of the inducer domain.

$$E_b = gH_2 - gH_1 \qquad (12)$$

We have reported in the same graph (Figure 5) the evolution of the specific energy supplied by the machine ψ_t as well as the specific energy transferred to the fluid ψ_b as a function of cavitation number ψ_c.

According to Figure 5, the drop of specific energy at ψ_c ~0.12 corresponds to a drop of both supplied and transferred energies. This observation evidences that the flow field is deeply changed as the cavitation extends beyond the throat region, leading to lower value of the torque. Nevertheless, the transferred energy decreases faster than the supplied energy, which demonstrates that the hydrodynamic losses due to cavitation development play a major role in the head drop phenomenon.

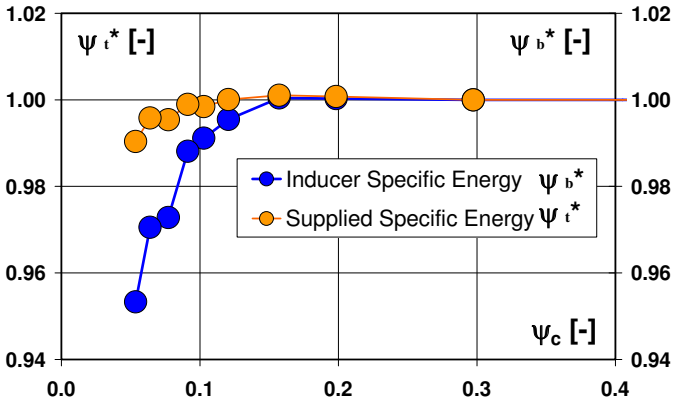

Figure 5 Evolution of the supplied and transferred specific energy coefficients vs. ψ_c

Blade-fluid transfer

In order to eliminate the fraction of pressure, which does not contribute to the torque, we may define the following coefficients for any given location M on the blade surface:

$$Cp_{t\_T}(M) = \frac{\vec{U}}{\|\vec{U}\|} \cdot \vec{n}\, Cp_t(M) \qquad (13)$$

$$Cp^*_{t\_T}(M) = \left[\frac{\vec{U}}{\|\vec{U}\|} \cdot \vec{n}\, Cp_t(M)\right]_{pressure\ side} + \left[\frac{\vec{U}}{\|\vec{U}\|} \cdot \vec{n}\, Cp_t(M)\right]_{suction\ side} \qquad (14)$$

where $\vec{U}$ is the peripherical velocity and $\vec{n}$ the normal to the blade surface at location M.

We have plotted Figure 6 the distribution of the coefficient $Cp^*_{t\_T}$ for both cavitation free condition and cavitation condition ψ_c = 0.054. We have also presented Figure 7 the coefficient Cp_{t_T} evolution along the blade chord for both 0.1 and 0.9 span values.

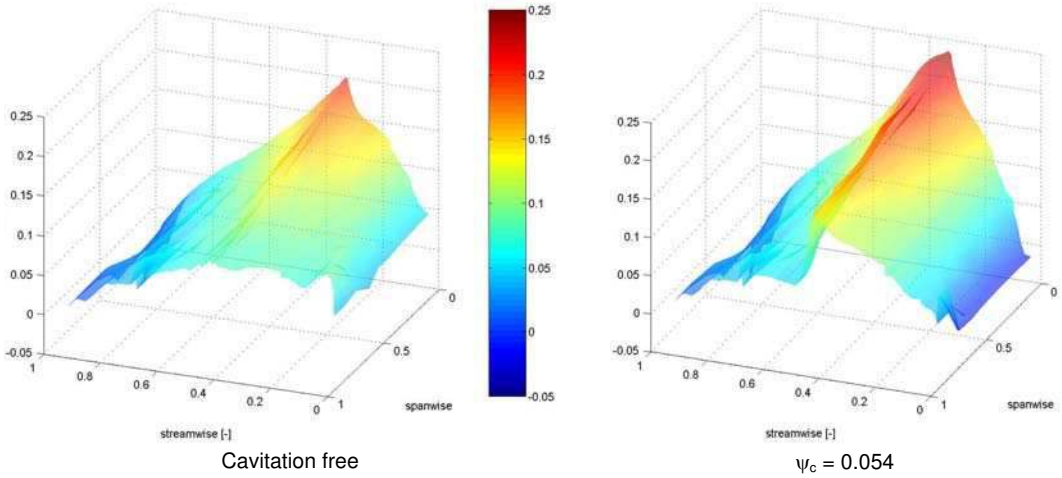

Figure 6 $Cp^*_{t\_T}$ distribution on the inducer blade

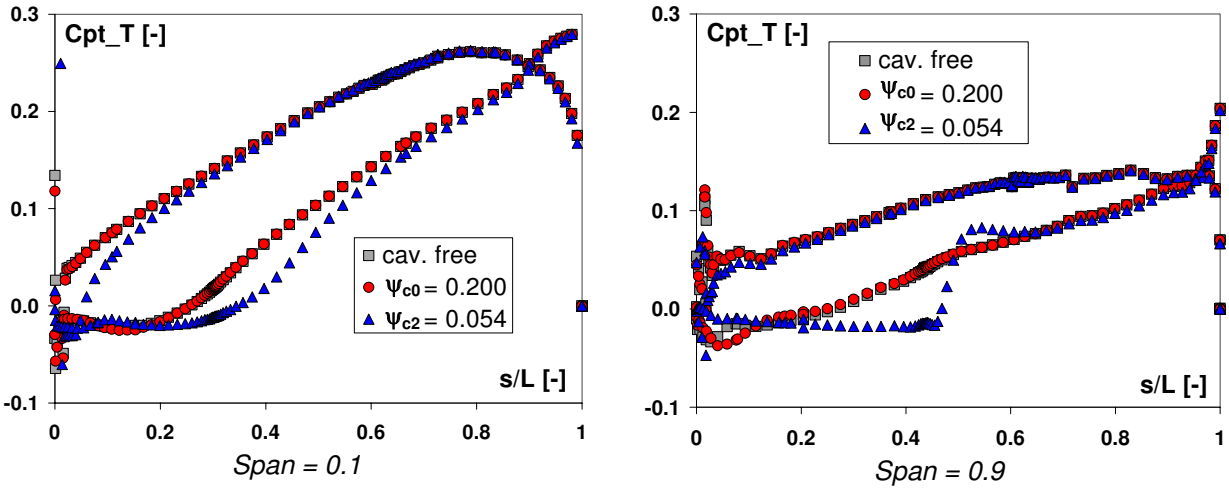

Figure 7 Evolution of Cp_{t_T} coefficient on the blade near the hub and the shroud areas

As the cavitation parameter is decreased, one may easily observe a decrease of $Cp^*_{t\_T}$ coefficient in the leading edge area followed by an increase of the same coefficient at the cavity closure zone. Since no alteration of the torque is observed for ψ>0.12, the loss and gain in $Cp^*_{t\_T}$ coefficient are almost balanced. As soon as the cavity reaches the throat, the resulting drop of the torque illustrates that the loss in $Cp^*_{t\_T}$ coefficient is no more balanced by the gain at the cavity closure. Furthermore, one may easily observe in Figure 7 that the occurrence of leading edge cavitation on the pressure side is due to a significant decrease of pressure coefficient in this area. This illustrates once again the modification of the flow field in the channel as soon as the main cavitation reaches the throat area. The cavitation in pressure side could be the reason of the torque loss.

Conclusion

In the present study, a multiphase CFD methods for cavitation modeling have been investigated in the case of 3-bladed industrial inducer. Computation analysis and experimental comparison allowing the validation of the model have been done.

The model allows a good prediction of the cavitation inception, the main cavity dimensions, as well as the threshold corresponding to the head drop is also well predicted. The cavitation induced head drop is mainly due to an increase of energy losses. A secondary reason of the head phenomenon is a decrease of the supplied energy resulting from a torque reduction.

The hydrodynamic mechanism of head drop is investigated through a global and local analysis of the flow field. As soon as the leading edge cavitation reaches the throat, it causes a flow blockage. The lack of the velocity in the flow direction in the cavity wake is balanced by an increase of the velocity in the hub region. Although this flow imbalance is mitigated further in the channel, the flow does not recover completely. The pressure distribution in the pressure side is significantly reduced at the leading edge, which allows cavitation occurrence and thereby influences the energy transfer.

Although this analysis provides an explanation of the hydrodynamic origin of the head drop; it should be noticed that absolute value of head drop is not well predicted. In fact, the actual solution of the flow is steady-state and the flow rate is fixed in the computation which is far form the realistic pumping systems where the cavitation may induce significant flow unsteadiness and large fluctuation of the cavity length as well as the flow rate.

Acknowledgments

Authors would like to thank the Swiss Center for Scientific Computing for their valuable help and computing facilities. They are also grateful to the Swiss National Science Foundation, grant award No FN-21-63842.00/1, as well as Mitsubishi Heavy Industry R&D Centre for their financial support.

References

Ref 1 Lakshminarayana B., 1982, “Fluid Dynamics of Inducers. A Review”, ASME JFE 4. pp 411-427.

Ref 2 Kueny J. L., Desclaux J., 1989, “ Theoritical Analysis of Cavitation in rocket Engine Inducers ”, ASME Pumping Machinery Symposium, San Diego.

Ref 3 Hirschi R., Dupont F., Avellan F., 1998, “Centrifugal Pump Performance Drop Due to Leading Edge Cavitation: Numerical Predictions Compared With Model Tests”, J. Fluids Eng., vol.120, pp 705-711.

Ref 4 Y. Tsujimoto, K. Kamijo, Y. Yoshida, 1993, “A Theoritical Analysis of Rotating Cavitation in Inducers”, Journal of Fluid Engineering, Vol. 115 pp.135-141

Ref 5 Franc J. P., Avellan F, Belahadji B, Billard JY, Briancon-Marjollet L, Frechou D, Fruman D. H., Karimi A., Kueny J. L., Michel J. M., 1995, " La Cavitation, Mecanismes Physiques et Aspects Industriels" Presses Universitaires de Grenoble, France.

Ref 6 CFX-TASCflow, V 2.12, AEA Technology, Canada, 2000.

Ref 7 H. Horigushi, S. Watanabe, Y. Tsujimoto, 2000, "Theoritical Analysis of Cavitation in Inducers With Unequal Blades With Alternate Leading Edge Cutback" JFE 412 pp 412-424

Ref 8 Medvitz, R. B., Kunz, R. F., Boger, B. A., Lindau, mJ. W., Yocum, A. M., Pauley L. L., 2001, "Performances analysis of cavitating flow in centrifugal pumps using multiphase CFD", 2001 ASME Fluids Eng. Conf. , May 29 - June 1, 2001, New Orleans, Louisiana.

Ref 9 Singhal A. K., Athavale M. M., Li H., Jiang Y., 2002, "Mathematical Basis and Validation of the Full Cavitation Model", J. Fluids Eng., Vol. 124, pp 617-624, 2002.

Ref 10 Aït Bouziad Y., Guennoun F., Farhat M., Avellan F., 2002, "Numerical Simulation of Leading Edge Cavitation". Proceedings of FEDSM'03 4th ASME-JSME Joint Fluids Engineering Conference, Honolulu, Hawaii, USA, July 6-11 2003. FEDSM2003-45312.

Ref 11 Guennoun Faiçal, Farhat Mohamed, Aït Bouziad Youcef, Avellan François, "Experimental Investigation of a Particular Traveling Bubble Cavitation" Fifth International Symposium on Cavitation (CAV2003) Osaka, Japan, November 1-4, 2003

Ref 12 Delgosha-Coutier O., R. Fortes Patella, J. L. Reboud , M. Hofmann, B. Stoffel 2003, "Experimental and Numerical Studies in a Centrifugal Pump With Two-Dimensional Curved Blades in Cavitating Condition", JFE vol 125, pp 970-979.